HHS Public Access

Author manuscript

Cell Rep. Author manuscript; available in PMC 2017 May 10.

Published in final edited form as:

Cell Rep. 2016 May 10; 15(6): 1202–1213. doi:10.1016/j.celrep.2016.04.007.

Targeted Delivery of Immunomodulators to Lymph Nodes

Jamil Azzi[1,7], **Qian Yin**[4,7], **Mayuko Uehara**[1,7], **Shunsuke Ohori**[1], **Li Tang**[4], **Kaimin Cai**[4], **Takaharu Ichimura**[1], **Martina McGrath**[1], **Omar Maarouf**[1], **Eirini Kefaloyianni**[1], **Scott Loughhead**[3], **Jarolim Petr**[5], **Qidi Sun**[4], **Mincheol Kwon**[4], **Stefan Tullius**[2], **Ulrich H. von Andrian**[3,6], **Jianjun Cheng**[4,*], and **Reza Abdi**[1,*]

[1]Transplantation Research Center, Renal Division, Brigham and Women's Hospital, Harvard Medical School, Boston, MA 02115, USA

[2]Division of Transplant Surgery and Transplant Surgery Research Laboratory, Brigham and Women's Hospital, Harvard Medical School, Boston, MA 02115, USA

[3]Department of Microbiology and Immunobiology, Harvard Medical School, Boston, MA 02115, USA

[4]Department of Materials Science and Engineering, University of Illinois at Urbana–Champaign, Urbana, IL 61820, USA

[5]Department of Pathology, Clinical Laboratories Division, Brigham and Women's Hospital, Harvard Medical School, Boston, MA 02115, USA

[6]The Ragon Institute of MGH, MIT, and Harvard, Cambridge, MA 02139, USA

SUMMARY

Active-targeted delivery to lymph nodes represents a major advance toward more effective treatment of immune-mediated disease. The MECA79 antibody recognizes peripheral node address in molecules expressed by high endothelial venules of lymph nodes. By mimicking lymphocyte trafficking to the lymph nodes, we have engineered MECA79-coated microparticles containing an immunosuppressive medication, tacrolimus. Following intravenous administration, MECA79-bearing particles showed marked accumulation in the draining lymph nodes of transplanted animals. Using an allograft heart transplant model, we show that targeted lymph node delivery of microparticles containing tacrolimus can prolong heart allograft survival with

*Correspondence: jianjunc@illinois.edu (J.C.), rabdi@rics.bwh.harvard.edu (R.A.).
[7]Co-first author

SUPPLEMENTAL INFORMATION

Supplemental Information includes two figures, one table, and one movie and can be found with this article online at http://dx.doi.org/10.1016/j.celrep.2016.04.007.

AUTHOR CONTRIBUTIONS

J.A. designed and performed experiments, analyzed and interpreted data, and drafted the manuscript. M.U. and S.O. performed microsurgery and analyzed and interpreted data. Q.Y., L.T., K.C., and J.C. contributed significantly to the chemical design of the polylactide-drug conjugates. Q.Y., L.T., K.C., O.S., and M.K. contributed significantly to the synthesis of the polylactide-drug conjugate and to the characterization of the polylactide-drug conjugates and the related nanoconjugates. Q.Y., L.T., K.C., and M.K. contributed significantly to the scaling up of the polylactide-drug conjugates for in vitro and in vivo studies. T.I. and J.P. performed experiments and analyzed data. S.T. and U.H.v.A. helped with the study design. J.C. and R.A. helped with the study design, interpreted data, and critically revised and finalized the manuscript.

negligible changes in tacrolimus serum level. Using MECA79 conjugation, we have demonstrated targeted delivery of tacrolimus to the lymph nodes following systemic administration, with the capacity for immune modulation in vivo.

Graphical Abstract

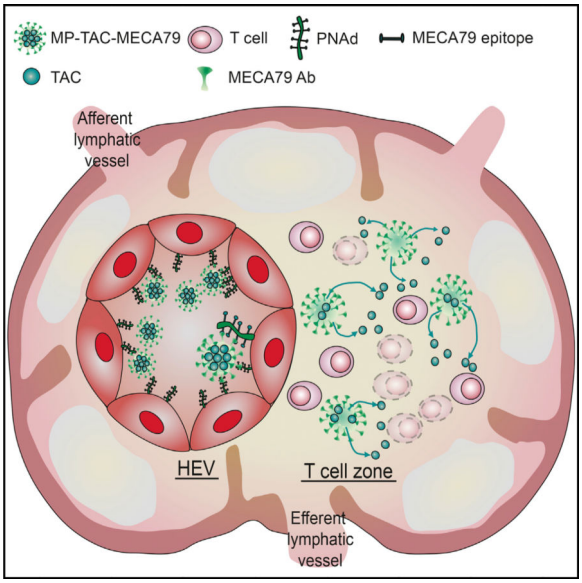

INTRODUCTION

Lymph nodes (LNs) function as a primary site for the priming and activation of immune cells in a wide variety of immune-mediated diseases (Goldstein et al., 2003; von Andrian and Mempel, 2003). Recognition of non-self alloantigens occurs in the draining lymph nodes (DLNs), resulting in the formation of alloreactive T cells and subsequent transplant rejection (Lakkis et al., 2000). Similarly, pancreatic lymph nodes play a key role in the formation of autoreactive T cells and in the pathogenesis of type 1 diabetes (Park and Kupper, 2015). LNs are also common sites for primary lymphoproliferative malignancies and metastatic niches (Stacker et al., 2014). Therefore, developing targeted delivery of drugs to the LNs represents a significant milestone and holds the potential to increase the efficacy of immune and cancer therapies. Targeted drug delivery also allows reduced systemic dosing with corresponding reductions in off-target toxicities.

The optimal, most clinically applicable drug delivery system would involve intravenous administration of an agent that would then localize to and act at a chosen site. In recent years, innovative approaches have been developed to target drugs specifically to the lymphoid system (Dane et al., 2011; Hunter et al., 2014; Jewell et al., 2011; Liu et al., 2014; Reddy et al., 2007; Yeste et al., 2012). Despite these advances, a LN-targeted drug delivery system using the intravenous route remains to be fully developed. Successful targeted delivery of immunoregulatory molecules or chemotherapy drugs to the LNs following intravenous administration holds immense potential for application in the treatment of a wide variety of immune-mediated diseases and cancers.

The primary concept behind our microparticle (MP) delivery system essentially shadows the footsteps of naive T cells and central memory cells, which circulate between the blood and LNs for antigen surveillance (von Andrian and Mackay, 2000). The trafficking of lymphocytes from the circulation to LNs is initiated by a highly regulated process referred to as tethering, which is controlled by selectin molecules (Somers et al., 2000). L-selectin, expressed on leukocytes, recognizes sulfated sialyl-Lewis^X-like sugars, called peripheral node addressins (PNAds), which are expressed by high endothelial venules (HEVs) in the LNs (Carlow et al., 2009; Sperandio et al., 2009; von Andrian and Mackay, 2000). Through this interaction, L-selectin plays a key role in the continuous homing of naive T cells to the LNs, where they encounter antigens presented by antigen-presenting cells. The monoclonal antibody (Ab) MECA79 binds PNAd, and, utilizing this interaction, we have successfully designed an innovative LN-targeted drug delivery strategy. Our platform consists of MECA79-bearing particles with the capacity to load and release tacrolimus (TAC). TAC is the most commonly clinically used immunosuppressant post-transplantation, and by directing this agent to the site of T cell activation in the lymph node, we have developed a functional, clinically relevant approach. Using a cardiac transplant model, we show proof of concept of the targeted delivery of MECA79-coated particles to DLNs, achieving immune modulation in vivo and resulting in improved heart allograft survival with negligible levels of TAC in peripheral blood.

RESULTS

Formulation of MP-TAC-MECA79

TAC was first conjugated to the poly(lactide) (PLA) polymer chain through TAC-initiated, controlled ring-opening polymerization (ROP) of lactide (LA) mediated by (BDI-EI)ZnN(TMS)$_2$, an organozinc catalyst (Figure 1; Chamberlain et al., 2001; Tong and Cheng, 2008). After TAC was mixed with 1.0 equivalent (BDI-EI)ZnN(TMS)$_2$, the in situ-formed (BDI-EI)Zn-TAC complex (Figure 1A) initiated and completed the polymerization of LA at room temperature (Figure 1B), resulting in TAC-PLA conjugate with a precisely controlled structure and molecular weight. The loading of TAC can thus be precisely controlled by adjusting monomer/initiator (LA/TAC) ratios. At the LA/TAC molar ratio of 25 (molar ratio, on a lactide basis), the drug loading of TAC-PLA conjugates can be as high as 18.3% with nearly 100% loading efficiency. After polymerization, TAC is covalently conjugated to the terminals of PLA through a hydrolysable ester linker, evidenced by the end group analysis via MALDI-TOF mass spectrometry (MS) (Figure 1C).

MECA79 monoclonal antibody-modified, TAC-loaded microparticles (MP-TAC-MECA79) were then prepared using the double emulsion method (Figure 1A). The synthesized TAC-PLA was first mixed with poly(ethylene glycol)-*b*-poly(lactic-*co*-glycolic acid) (PEG-PLGA) and PEG-PLA-carboxylic acid (COOH) and then emulsified in poly(vinyl alcohol) (PVA) solution using sonication and homogenization. The formed MPs with carboxyl groups were further conjugated with protein G by a coupling reaction and then bonded with MECA79. The resulting MPs had sizes of 2.30 ± 0.14 μm in diameter by dynamic light scattering (DLS) measurement (Figure 2A) and confirmed by scanning electron microscope imaging (Figure 2B). Non-modified MP-TAC was formulated by using the same method and

showed similar physicochemical properties as MP-TAC-MECA79 (Figure 2C). To facilitate potential clinical translation, it is desirable to formulate particles in solid form to minimize drug release prior to use. Thus, we attempted to use BSA as the lyoprotectant of MP solid formulation. The data in Figure 2D demonstrate that BSA could effectively protect the solid form of MP-TAC-MECA79 and MP-TAC from aggregation after reconstitution in water.

Immunosuppressive Capacity of MP-TAC-MECA79 In Vitro

We then examined the retention and release of TAC from MP-TAC-MECA79 by testing its ability to suppress T cell proliferation in vitro. MP-TAC-MECA79 and an equivalent dose of free TAC were added in a dose-dependent fashion to an anti-CD3/CD28 T cell stimulation assay. As shown in Figures 3A and 3B, MP-TAC-MECA79 and free TAC suppressed T cell proliferation, as measured by thymidine incorporation, in a dose-dependent fashion, starting at 0.5 ng/ml TAC-equivalent concentration ($p < 0.05$). Furthermore, MP-TAC-MECA79 suppressed inflammatory cytokine (interleukin-2 [IL-2], interferon γ [IFNγ], IL6, and IL17) production by T cells, as measured by Luminex analysis of the T cell culture supernatant (Figures 3C–3F). However, MP-MECA79 particles with no TAC (MP-MECA79 particles dose-equivalent to MP-TAC-MECA79 at 5 ng/ml TAC equivalent) did not suppress T cell proliferation when added to the anti-CD3/ CD28 T cell stimulation assay ($174.276\ 3\ 10^3 \pm 2.227 \times 10^3$ versus $155.587 \times 10^3 \pm 21.089 \times 10^3$, respectively; $p = 0.22$), demonstrating the requirement for the immunosuppressive agent tacrolimus to prevent T cell activation.

Targeted Delivery of MP-TAC-MECA79 to Draining Lymphoid Tissues Post-transplantation

PNAds are expressed on the vascular endothelium of peripheral LNs and are induced on venules at sites of chronic inflammation, including transplanted organs undergoing rejection (Baddoura et al., 2005; Michie et al., 1993; Xu et al., 2003; Yin et al., 2011). We first investigated the expression of PNAd in DLNs using a murine skin transplant model, which has a well-defined lymphatic drainage to the DLNs. C57BL/6 recipients were transplanted with full-thickness skin grafts taken from either C57BL/6 donors (syngeneic) or BALB/c donors (allogeneic), as described previously (Yuan et al., 2003). DLNs were retrieved from transplanted mice on day 7 post-transplantation. We then examined the level and pattern of expression of PNAd in DLNs by western blot and immunohistochemistry. As shown in Figure 4A, DLNs of allogeneic transplants had a significant increase in PNAd expression compared with syngeneic transplants. Following the normalization of ERK1/2 as the loading control, our densitometric analysis indicated a 4-fold increase in allogeneic hosts compared with syngeneic ones (Figure 4A; ***$p < 0.001$, $n = 3$ mice/group). Similarly, DLNs from allogeneic recipients showed a marked increase in PNAd-expressing vasculature compared with the non-draining LNs (Figures 4B and 4C).

We then tested the efficacy of preferential trafficking of MECA79-coated particles to DLNs following transplantation. We first synthesized TAC-containing particles coated with MECA79 (MP-TAC-MECA79) and non-coated (MP-TAC). Both sets of particles were labeled with rhodamine to monitor their trafficking (MP-Rhd-MECA79 and MP-Rhd, respectively) (Table S1). On day 7 after transplantation of an allogeneic skin graft, recipient mice were injected with either MP-Rhd-MECA79 or MP-Rhd via the tail vein. We harvested the DLNs 24 hr after injection and quantified the rhodamine-labeled particles using

immunohistochemistry. LN sections were stained for nuclei with DAPI (blue) and PNAd (green). These sections were examined for the presence of red MP-Rhd and MP-Rhd-MECA79 particles (rhodamine-loaded), and particles were counted per high-power field (403 objective). As shown in Figures 4D and 4E, immunohistochemistry staining showed a much higher number of particles in the DLNs of animals injected with MP-Rhd-MECA79 (red dots, Figure 4D, right) compared with MP-Rhd (Figure 4D, left). The MP-Rhd-MECA79 was localized adjacent to the PNAd-positive vessels and surrounding cells (Figure 4D, right).

Next, draining and non-draining LNs of skin allograft recipients treated with MP-Rhd-MECA79 were examined by two-photon microscopy. As shown in Figure 4F, a higher density of PNAd-positive vessels (green) was again observed in DLNs compared with non-draining LNs in addition to a higher number of MP-Rhd-MECA79 (red). Optical sections of the tissue imaged by two-photon microscopy were compiled into a three-dimensional volume (Movie S1).

A lower level of PNAd expression was observed in the non-draining LNs of transplanted mice compared with DLNs (Figures 4B and 4C). As predicted by this pattern of PNAd expression, no difference was observed in the trafficking of MP-Rhd-MECA79 and MP-Rhd particles to the non-draining LNs of transplant recipients, as assessed by flow cytometry (Figure S1A and S1C) or by immunohistochemistry (data not shown).

Spleens of transplanted mice were also analyzed by immunohistochemistry after intravenous injection of the different particles. No splenic PNAd staining was detected, as shown in Figure S2A. As expected, no difference in trafficking of MP-Rhd-MECA and MP-Rhd particles to the spleens of transplanted mice was detected by flow cytometry analysis, as shown in Figure S2B and S2C (n = 4 mice/group).

Functional Role of MECA79 in Targeted Trafficking of MP-TAC-MECA79 Particles

To show the functional role of the MECA79 Ab in mediating the preferential trafficking of MP-Rhd-MECA79 to the DLNs, on day 7 after transplantation, skin allograft recipients were injected with anti-PNAd blocking antibody (MECA79, 200 μg/mouse) 1 hr before injection of MP-Rhd-MECA79 or MP-Rhd. DLNs were isolated, and cell suspensions were analyzed by flow cytometry to detect the rhodamine-labeled particles. In the absence of PNAd blockade, significantly more of rhodamine-labeled particles were detected by flow cytometry in the inguinal DLNs of mice injected with MP-Rhd-MECA79 compared with MP-Rhd (1,527 ± 480 versus 185.8 ± 57 particles, respectively; $p < 0.05$; n = 3–4 mice/group) (Figures 5A and 5C). Blocking PNAd reduced the trafficking of MP-Rhd-MECA79 to the DLNs (1,527 ± 480 versus 98 ± 56 particles, respectively; $p < 0.05$; n = 3–4 mice/group). However, PNAd blockade did not affect the observed low levels of MP-Rhd trafficking to the DLNs (185.8 ± 57 versus 193 ± 71 particles, respectively; p = not significant [ns]; n = 3–4 mice/group) (Figures 5B and 5C). This shows that the preferential trafficking of MP-Rhd-MECA79 to DLNs after transplantation is mediated by the binding of MECA79 to LN-expressed PNAd.

To assess the accumulation of particles in other lymphoid tissues, non-draining LNs (pancreatic LNs) were isolated, and cell suspensions were analyzed by flow cytometry to detect rhoda-mine-labeled particles under PNAd blockade. The presence or absence of PNAd blockade had no effect on the accumulation of intravenously injected MP-Rhd-MECA79 or MP-Rhd in non-draining lymph nodes (Figure S1A–S1C). After allogeneic transplantation, draining lymph nodes enlarge markedly because of allostimulated lymphocyte proliferation. As anticipated, more than 10-fold more cells were isolated from DLNs than non-draining lymph nodes, as measured by flow cytometry (Figure S1D). This effect leads to the observed substantial differences in absolute cell count despite a similar overall percentage, as seen by flow cytometry analysis.

Therapeutic Efficacy of MP-TAC-MECA79 in Prolonging Heart Allograft Survival

To examine the therapeutic efficacy of MP-TAC-MECA79 in a more clinically applicable solid organ transplant model, we next analyzed the expression of PNAd in the draining and non-draining LNs of heart transplant recipients. As shown in Figure 6A, immunohistochemistry analysis of DLNs of mice transplanted with heart allografts showed a significant increase in PNAd expression compared with non-draining LNs on day 7 post-transplantation. Furthermore, a newly formed network of PNAd-positive cells from much larger vessels in the DLNs was also observed (arrows). To study allograft survival, C57BL/6 recipients of BALB/c hearts were injected daily with MP-TAC-MECA79, MP-TAC, or free TAC (each dosed at 1 mg/kg TAC equivalent) for 6 consecutive days. Given that high serum levels of TAC cause allograft vascular injury and toxicity, we were interested in the effect of our treatment particles on systemic TAC exposure. To assess this, we measured the blood levels of TAC in transplanted mice on day 3 after transplantation (Azzi et al., 2010; Chapman and Nankivell, 2006; Vercauteren et al., 1998; Wong et al., 2005). As shown in Figure 6B, the TAC peak level 2 hr after injection of the compounds was significantly lower in the MP-TAC-MECA79 compared with the free TAC group (2.63 ± 0.56 versus 37.00 ± 2.62, respectively; $p < 0,05$; n = 3 mice/group). Furthermore, as shown in Figure 6C, the TAC trough level 24 hr after injection was also significantly lower for MP-TAC-MECA79 compared with free TAC (2.45 ± 0.05 versus 0.60 ± 0.05, respectively; $p < 0.05$; n = 3 mice/group). No significant difference was seen in the peak and trough levels of TAC in MP-TAC-MECA79 and MP-TAC (Figures 6B and 6C).

Interestingly, despite a more than 15-fold decrease in the peak level of TAC, transplanted mice treated with MP-TAC-MECA79 showed a significant prolongation of heart allograft survival compared with control groups (median survival 11 days versus 7 days, respectively; $p < 0.05$; n=4–5/group). Furthermore, heart allograft recipients treated with MP-MECA79 (without TAC) or MP (without TAC) showed no increase in allograft survival compared with untreated mice or mice treated with MP-TAC or free TAC (median survival 7 days, p = ns, n = 4–5/group) (Figure 6D). These data confirm that the allograft-prolonging effect is dependent on the presence of TAC within microparticles delivered to DLNs.

Finally, we measured the suppressive effects of MP-TAC-MECA79 on activated T cells in the DLNs of treated animals. Activated alloreactive T cells are identified by their upregulated expression of CD44 and downregulation of CD62L. These

$CD4^+CD62L^{low}CD44^{high}$ T cells only require low levels of antigenic stimulation to undergo substantial proliferation and are the effector population in allograft rejection (Azzi et al., 2015; Jones et al., 1999; Krupnick et al., 2014; Vergani et al., 2013). On day 7, mice were harvested, and the DLNs of heart allograft recipients were analyzed by flow cytometry. CD4 effector T cells ($CD4^+CD62L^{low}CD44^{high}$) were significantly reduced in mice treated with MP-TAC-MECA79 compared with the MP-TAC- and free TAC-treated groups (271.0 ± 65.00 versus 1,686 ± 361.9 versus 4,508 ± 735.5, respectively; $p < 0.05$; n = 3 mice/group) (Figures 6E and 6F).

DISCUSSION

The potential for targeted drug delivery to improve the efficacy/ safety ratio of existing drugs has fueled considerable research and prompted clinicians to apply this technology across a range of clinical settings (Wagner et al., 2006). However, targeted delivery to specific tissue sites following systemic administration remains challenging (Mitragotri et al., 2014). The primary focus of our work has been to achieve active-targeted delivery to the HEVs of LNs via an intravenous route. The DLN is a primary site of alloreactive and autoreactive T cell activation and therefore plays a central role in the pathogenesis of transplant rejection and autoimmune diseases, rendering this site an attractive target for drug delivery (Lakkis and Sayegh, 2003; Park and Kupper, 2015).

Solid organ transplantation is a life-saving procedure for end organ failure, but its success is blunted by the limitations of currently available immunosuppressive agents. Calcineurin inhibitors such as TAC are the cornerstone of immunosuppressive therapy after transplantation. However, TAC-induced organ toxicity, cardiovascular events, and malignancies are major causes of graft loss and mortality (Halloran, 2004). There have been numerous sizable clinical trials targeted at sparing, minimizing, or withdrawing calcineurin inhibitors in an attempt to reduce their toxicity. However, these trials have faced significant challenges, including decreased efficacy, persistent toxicities, and new toxicities caused by the replacement drug (Flechner et al., 2008; Haller and Oberbauer, 2009). Therefore, developing innovative strategies to improve the ratio of efficacy and toxicity of immunosuppressive therapies remains one of the greatest challenges in the treatment of immune-mediated diseases, including transplant rejection (Azzi et al., 2013). Given that nano-therapeutics are already in clinical use, this platform has the potential to tackle one of the most immediate clinical problems in transplantation.

Migration of naive lymphocytes to the LNs is initiated by the interaction of L-selectin expressed on lymphocytes with a series of glycoprotein ligands expressed by HEVs in the lymph nodes, referred to as PNAd molecules (Berg et al., 1992; Butcher and Picker, 1996; Campbell et al., 2003; Hänninen et al., 1996; Michie et al., 1993; Streeter et al., 1988; van Zante et al., 2003). Following transplantation, we observed increased PNAd expression in DLNs. PNAds are recognized by the MECA79 monoclonal antibody, and, by engineering MECA79-coated microparticles, we sought to exploit the role of PNAd in lymphocyte trafficking in a model of transplant rejection. Our data indicate that MECA79 surface-bearing particles showed significantly greater trafficking to DLNs compared with control particles. We demonstrated significantly less accumulation of microparticles in non-draining

LNs where PNAd expression was unchanged. To show the functionality of MECA79, we blocked the interaction of MECA79 with PNAd prior to injection of particles, which abrogated targeted delivery to DLNs. Furthermore, MECA79-conjugated and -non-conjugated particles traffic equally to the spleen, which does not express PNAd. These data indicate that the marked increase in PNAd expression in the DLNs following transplantation drives the increased trafficking of MECA79-bearing particles to that site. This suggests that our targeted delivery system should be applicable to other disease states where PNAd is upregulated, highlighting its potential to treat a broad spectrum of diseases.

Although a skin transplant model with clear lymphatic drainage to DLNs was used to show proof of concept of targeted delivery, we then used a heart transplant model as a clinically applicable model to show proof of concept of efficacy. We used TAC-loaded particles because of TAC's importance as a clinical agent in the prevention of transplant rejection. Within the lymph node, MECA79-conjugated MPs with TAC reduced T cell proliferation, as evidenced by the marked reduction in $CD44^{high}CD62L^{low}$ activated alloreactive T cells in the DLNs of treated animals. At the molecular level, TAC inhibits calcineurin, which is responsible for the dephosphorylation of nuclear factor of activated T cells (NFAT). NFAT increases the activity of IL-2 and other cytokine-encoding genes (Azzi et al., 2013; Kolata, 1983; Zhang et al., 1996). Blockade of this pathway therefore prevents T cell activation and proliferation. Furthermore, peak TAC levels are closely correlated with the development of toxicities, and serum drug levels are readily quantifiable, allowing us to demonstrate both the efficacy of this directed therapy but also its considerable potential to decrease unwanted effects by minimizing total drug exposure. Indeed, treatment of allograft recipients with MP-TAC-MECA79 induced higher allograft survival compared with the other groups with markedly lower levels of TAC (>15-fold less) in peripheral blood. It is important to note that the extent of prolongation of graft survival reported here is based on using a single immunosuppressive agent, TAC, which does not induce tolerance on its own in any transplant setting. Given that we used a stringent model of alloreactivity with a complete major histocompatibility complex (MHC) mismatch and achieved negligible TAC levels in peripheral blood, the observed prolongation of heart allograft survival represents a major immunomodulatory effect in vivo. These findings show the ability of this platform to achieve a greater degree of therapeutic efficacy while holding the potential to improve the side effect profile through reduced systemic drug exposure.

L-selectin itself is a rolling receptor because of its very short bonding time and inefficient accumulation. We chose a MECA79-based platform because MECA79 is likely to have broader coverage and also carries the advantage of blocking lymphocyte trafficking. MP-MECA79 without TAC showed no prolongation of graft survival, indicating that impaired lymphocyte homing because of PNAd blockade is unlikely to be a significant contributor to the observed graft survival. Furthermore, of all experimental groups, only MP-TAC-MECA79 showed prolongation of allograft survival, indicating dependence upon the local activity of TAC within the LNs to mediate this effect. With standard tools, it is impractical to compartmentalize TAC in the DLNs. In future studies, we foresee using evolving cutting edge matrix laser dissection methods, which may allow better analysis of the kinetics of targeted drugs in a very small environment such as the LNs.

There have been major efforts to build lymphatic delivery platforms for a wide variety of therapeutic and diagnostic applications. Many of these strategies use lymphatic absorption with promising results (Cho and Lee, 2014; Dane et al., 2011; Hunter et al., 2014; Jewell et al., 2011; Liu et al., 2014; Reddy et al., 2007; Yeste et al., 2012; Zhang and Lu, 2014). Our strategy, which targets HEVs via the intravenous route, could effectively complement these approaches and/or expand the therapeutic applications when targeting the lymphatic system.

The PNAd/L-selectin pathway has also been shown to regulate lymphocyte trafficking to lymphoid tissue in non-obese diabetic (NOD) mice (Xu et al., 2010). PNAd is upregulated on the venous endothelium in inflammatory states and autoimmune diseases such as type 1 diabetes mellitus (Michie et al., 1993; Mikulowska-Mennis et al., 2001; Penaranda et al., 2010). Therefore, it is likely that increased PNAd expression, similar to what we describe after transplantation, also occurs in the DLNs of tissues affected by autoimmunity.

Our drug delivery platform carries considerable inherent plasticity and could be re-engineered to incorporate a wide variety of immunoregulatory molecules and antibodies. Therefore, we envisage that this platform has the potential to deliver combinatorial therapies not only for the purpose of suppressing alloor auto-reactive T cells but also promoting regulatory T cells (Ochando et al., 2005). A number of studies have shown that particles in the micrometer range (such as ours, at 2–5 μm) accumulate readily within the lung capillary bed and are removed by the macrophage phagocytic system (MPS) of the spleen and liver (Blanco et al., 2015; Cabral et al., 2011; Kobayashi et al., 2014; Nel et al., 2009; Oussoren and Storm, 2001). One of our central future goals is to further improve the efficacy of this platform by designing smaller-size particles. Reducing the size of particles (~100 nm) would allow them to evade lung entrapment and avoid rapid clearance by the MPS, leading to a longer circulation time and therefore increased delivery to LNs (Blanco et al., 2015). Last, the use of protein G and BSA to coat particles may be associated with an adverse immune reaction when nano-formulations are used in humans. In the future, we aim to test other coating materials, such as branched PEG to increase PEG density on surface, zwitterionic materials that have shown interesting stealth effects, or human serum albumin. These materials will address the immunogenic effect of BSA and allow the conjugation of MECA79 (without protein G) with the surface coating.

Here we describe a drug delivery platform with the capacity to deliver drugs to the LNs in a targeted manner after intravenous administration, leading to in vivo immunomodulation with minimal detectable peripheral drug levels. With the capability to deliver a range of immunoregulatory molecules, this system has the potential to increase the efficacy of treatment for autoimmune disorders (i.e., delivering immunomodulatory molecules to the pancreatic lymph nodes for type 1 diabetes) (Park and Kupper, 2015) and a range of cancer therapies where the LN is an important site for disease progression (Stacker et al., 2014).

EXPERIMENTAL PROCEDURES

General

D,L-Lactide was purchased from TCI America, recrystallized three times in toluene, and stored at −30°C in a glove box prior to use. (BDI-EI)ZnN$(TMS)_2$ was prepared by following

reported procedures (Chamberlain et al., 2001). FK506 (TAC) (Cayman Chemical) was used as received. All other chemicals were obtained from Sigma-Aldrich and used as received unless otherwise noted. High-performance liquid chromatography (HPLC) analysis was performed on a System Gold system (Beckman Coulter). Infrared spectra were recorded on a PerkinElmer 100 serial Fourier transform infrared spectroscopy (FT-IR) spectrophotometer. MALDI-TOF MS spectra were collected on an Applied Biosystems Voyager-DETM STR system. The sizes and polydispersities of MPs were determined on a ZetaPALS dynamic light-scattering detector. The ζ potential of freshly prepared MPs was evaluated by Malvern Zetasizer. Lyophilization of MPs was completed on a benchtop lyophilizer (Freezone 2.5, Fisher Scientific. The sizes of MPs were characterized on a Hitachi S4700 high resolution scanning electron microscope.

Synthesis and Characterization of FK506-PLA Polymer Conjugate

(BDI-EI)ZnN$(TMS)_2$ (6.5 mg, 0.01 mmol) was dissolved in anhydrous tetrahy-drofuran (THF) (500 μl). The solution was added to a vial containing TAC (8.0 mg, 0.01 mmol), and the mixture was completely stirred for 15 min. LA (36.0 mg, 0.25 mmol) was dissolved in a vial containing THF (800 μl) and added to the mixture of TAC/(BDI-EI)ZnN$(TMS)_2$. FT-IR was used to follow the conversation of LA in the polymerization solution by monitoring the intensity of the lactone band at 1772 cm^{-1}. After LA was completely consumed, the polymerization was quenched by ice-cold methanol (20 μl). Then the polymer conjugate TAC-PLA was precipitated with ether (50 ml) and dried under a vacuum. The resulting TAC-PLA was denoted as TAC-PLA_n, where n is the monomer/initiator (LA/TAC) molar ratio. The polymer was then analyzed by MALDI-TOF mass spectrometry.

Preparation of MP-TAC-MECA79

TAC-MPs were prepared using the water-in-oil-in-water (W/O/W) solvent evaporation procedure (also known as the double emulsion method). In brief, 50 μl aqueous solution was emulsified in a mix of 1 ml solution of PEG-PLGA (30 mg), PLA-PEG-COOH (6 mg), and TAC-PLA (30 mg containing 5.5 mg TAC) in dichloromethane (DCM) using a probe sonicator (Sonic & Materials) at 10 W (1%) for 15–30 s. The emulsion was then poured into 50 ml of aqueous PVA (1%) aqueous solution, and the mixture was homogenized for 1 min at 8,000 rpm. The resulting emulsion was poured into 300 ml of aqueous PVA (0.3%) with gentle stirring, after which the organic solvent was evaporated by stirring at room temperature (RT) for 3 hr in the hood. The MPs were isolated by centrifugation at 10,000 rpm for 20–30 min, washed with distilled (DI) water (20 ml), and dispersed in DI water (20 ml). To modify the MP surface with MECA79 Ab, 1-ethyl-3-(3-dimethylaminopropyl)carbodiimide (10 mg) and N-hydroxysuccinimide (6 mg) were added to 20 ml MP solution (66 mg), followed by addition of protein G (0.5 mg in 40 μl DI water) after 10 min (Tong et al., 2010). The mixture reacted overnight at RT. The MP was then centrifuged at 10,000 rpm for 20 min, washed with DI water (20 ml), and dispersed in 20 ml DI water. The concentration of MECA79 Ab is 200 μg/ml. 50 μl of Ab solution was added into MP solution.

The MP was then washed as described above and dispersed in DI water for use. The MPs without added IgM during the formulation were used as a control (MP-TAC). The MP size was determined by DLS and scanning electron microscopy.

For the preparation of Rhd-labeled MP-Rhd or MP-Rhd-MECA79, Rhd-PLA (30 mg) was mixed with the DCM solution of the PEG-PLGA and PLA-PEG-COOH polymer for subsequent double emulsion. The resulting fluorescent MPs were collected and washed similarly.

ξ Potential Measurements

The ξ potential of the MPs was determined with a Malvern Zetasizer. The freshly prepared MPs were dispersed in DI water to a concentration of 0.5 mg/ml.

Lyophilization of MPs in the Presence of BSA as a Lyoprotectant

BSA as a lyoprotectant was added to the concentrated MP suspension at a mass ratio of BSA/MP =10/1. The solution was then lyophilized to dry powder, which was stored at −20°C prior to use. The MPs were reconstituted with water and stirred for 5 min. The sizes of the resulting NPs were analyzed by DLS.

Mice

C57BL/6 and BALB/c(H-2^d) mice were obtained from The Jackson Laboratory. All animals were used at 6–10 weeks of age (20–25 g) and housed in accordance with institutional and NIH guidelines. The Harvard Medical School Animal Management Committee approved all animal experiments.

Murine Skin Transplantation

Full-thickness trunk skin grafts (1 cm^2) harvested from BALB/c donors were transplanted onto the flanks of C57BL/6 recipient mice, sutured with 6.0 silk, and secured with dry gauze and a bandage for 7 days. The draining LN harvested was the inguinal LN. To count the absolute number of Rd-labeled particles in LNs, LN samples were prepared into single-cell suspension, and the cell number was enumerated by flow cytometry. The percentage of Rd-labeled events was measured by flow cytometry. This percentage was then applied to the count measured from the LN single-cell suspension, and the absolute count for Rd-labeled events was calculated.

Murine Cardiac Transplantation

Vascularized intra-abdominal heterotopic transplantation of cardiac allografts was performed using microsurgical techniques (Corry, 1973). Graft survival was assessed by daily palpation. Rejection was defined as complete cessation of cardiac contractility as determined by direct visualization and was confirmed by histological examination. Para-aortic lymph nodes from the host were harvested as draining LNs of the heart allografts.

Immunohistochemistry

Lymph node, spleen, lung, and liver tissue samples were snap-frozen with optical cutting temperature compound (OCT) in liquid nitrogen and stored at −70°C until use. Frozen sections (8 μm) were prepared using a cryostat and immediately used or stored at −70°C until use. The sections were fixed with ice-cold acetone for 1 min, washed with PBS for 10 min, and blocked for 30 min with 3% BSA-PBS as a blocking solution. The anti-HEV marker PNAd-Alexa Fluor 488 and anti-B cell B220-APC antibodies (eBioscience) were diluted (1:200) in the blocking solution. Sections were incubated with these antibodies for 1 hr at room temperature or overnight at 4°C. Sections were washed with PBS. After washing, a coverslip was placed with Vectorshield (Vector Laboratories) mounting medium containing DAPI, and sections were analyzed using a Nikon C1 laser confocal microscope. For negative controls, the sections were stained by omitting the primary antibody.

Two-Photon Microscopy—Draining and non-draining LNs from recipients of an allogeneic skin graft were frozen in OCT, and 200-μm sections were generated. Optical sections of the tissue were imaged by two-photon microscopy and compiled into a three-dimensional volume.

Western Blot

Lymph nodes were lysed in ice-cold lysis buffer, and the protein concentration of cell lysates was measured using the Bradford (Bio-Rad) assay. Equal amounts of protein were separated by 10% SDS-PAGE and transferred to a nitrocellulose membrane. The membranes were blocked with 5% non-fat milk in Tris-buffered saline (TBS)-0.05%Tween (TBST) and incubated overnight at 4°C with the following primary antibodies: MECA79 (anti-PNAd, BD Biosciences) and ERK1 (Santa Cruz Biotechnology). The blots were washed and developed with SuperSignal West Pico or West Dura chemiluminescent substrates (Thermo Scientific) using a Bio-Rad ChemiDoc imaging system, and the bands were quantified using Image Lab (Bio-Rad) software. MECA79 is a carbohydrate epitope found on a group of sulfation-decorated sialomucins, including sulfated ligands for CD62L (CD34, GlyCAM-1, Sgp200, and a subset of MAdCAM-1). This set of antigens has been referred to as PNAd with a molecular mass of 50–250 kD. Therefore, in the western blot, bands of multiple molecular weights were detected.

Flow Cytometric Analysis

Cells recovered from spleens and peripheral lymphoid tissues were analyzed by flow cytometry with a FACS Canto-II flow cytometer (BD Biosciences) and analyzed using FlowJo software version 9.3.2 (Tree Star).

Anti-CD3/CD28 Stimulation Assay

100 μl of anti-CD3 Ab diluted in PBS (1 μg/ml, BD Biosciences) was added to each well of a 96-well flat-bottom plate, placed at 37°C for 4 hr, and then washed twice with PBS. Soluble anti-CD28 Ab (1 μg/ml, BD Biosciences) was added to each well in the presence of 5×10^5 splenocytes and an increasing concentration of MP-TAC-MECA79. Cultures were pulsed with triturated thymidine 72 hr after stimulation to assess cell proliferation.

Luminex Assay—A 21-plex cytokine kit (Millipore) was used according to the manufacturer's instructions.

Statistics—Kaplan-Meier survival graphs were constructed, and a log-rank comparison of the groups was used to calculate *p* values. Unpaired t test was used for comparison of experimental groups. Differences were considered to be significant for $p \leq 0.05$. Prism software was used for data analysis and drawing graphs (GraphPad). Data represent mean ± SEM.

Supplementary Material

Refer to Web version on PubMed Central for supplementary material.

Acknowledgments

This work was supported by an American Heart Association grant (to J.A.), the National Institute of Allergy and Infectious Diseases of the NIH under Award RO1AI091930 (to R.A.), and the NIH Director's New Innovator Award 1DP2OD007246 (to J.C.). The synthesis of the polylactide-drug conjugates and nanoconjugates was partially supported by NSF-CHE-1308485. This research was also supported in part by a gift from Mr. Matthew S. Forelli. U.H.v.A. was supported by funds from the HMS Center for Immune Imaging and the Ragon Institute and by NIH grants AI112521, AI111595, and AR068383. Q.Y. was funded at the University of Illinois at Urbana—Champaign by NIH National Cancer Institute Alliance for Nanotechnology in Cancer (Midwest Cancer Nanotechnology Training Center) (R25 CA154015A). The synthesis of the polylactide-drug conjugates and nanoconjugates was partially supported by NSF-CHE-1308485.

REFERENCES

Azzi J, Tang L, Moore R, Tong R, El Haddad N, Akiyoshi T, Mfarrej B, Yang S, Jurewicz M, Ichimura T, et al. Polylactide-cyclosporin A nanoparticles for targeted immunosuppression. FASEB J. 2010; 24:3927–3938. [PubMed: 20547662]

Azzi JR, Sayegh MH, Mallat SG. Calcineurin inhibitors: 40 years later, can't live without. J. Immunol. 2013; 191:5785–5791. [PubMed: 24319282]

Azzi J, Ohori S, Ting C, Uehara M, Abdoli R, Smith BD, Safa K, Solhjou Z, Lukyanchykov P, Patel J, et al. Serine protease inhibitor-6 differentially affects the survival of effector and memory alloreactive CD8-T cells. Am. J. Transplant. 2015; 15:234–241. [PubMed: 25534448]

Baddoura FK, Nasr IW, Wrobel B, Li Q, Ruddle NH, Lakkis FG. Lymphoid neogenesis in murine cardiac allografts undergoing chronic rejection. Am. J. Transplant. 2005; 5:510–516. [PubMed: 15707405]

Berg EL, Magnani J, Warnock RA, Robinson MK, Butcher EC. Comparison of L-selectin and E-selectin ligand specificities: the L-selectin can bind the E-selectin ligands sialyl Le(x) and sialyl Le(a). Biochem. Bio-phys. Res. Commun. 1992; 184:1048–1055.

Blanco E, Shen H, Ferrari M. Principles of nanoparticle design for overcoming biological barriers to drug delivery. Nat. Biotechnol. 2015; 33:941–951. [PubMed: 26348965]

Butcher EC, Picker LJ. Lymphocyte homing and homeostasis. Science. 1996; 272:60–66. [PubMed: 8600538]

Cabral H, Matsumoto Y, Mizuno K, Chen Q, Murakami M, Kimura M, Terada Y, Kano MR, Miyazono K, Uesaka M, et al. Accumulation of sub-100 nm polymeric micelles in poorly permeable tumours depends on size. Nat. Nanotechnol. 2011; 6:815–823. [PubMed: 22020122]

Campbell DJ, Kim CH, Butcher EC. Chemokines in the systemic organization of immunity. Immunol. Rev. 2003; 195:58–71. [PubMed: 12969310]

Carlow DA, Gossens K, Naus S, Veerman KM, Seo W, Ziltener HJ. PSGL-1 function in immunity and steady state homeostasis. Immunol. Rev. 2009; 230:75–96. [PubMed: 19594630]

Chamberlain BM, Cheng M, Moore DR, Ovitt TM, Lobkovsky EB, Coates GW. Polymerization of lactide with zinc and magnesium beta-diiminate complexes: stereocontrol and mechanism. J. Am. Chem. Soc. 2001; 123:3229–3238. [PubMed: 11457057]

Chapman JR, Nankivell BJ. Nephrotoxicity of cyclosporin A: short-term gain, long-term pain? Nephrol. Dial. Transplant. 2006; 21:2060–2063. [PubMed: 16728428]

Cho HY, Lee YB. Nano-sized drug delivery systems for lymphatic delivery. J. Nanosci. Nanotechnol. 2014; 14:868–880. [PubMed: 24730304]

Corry AM. 1973 meeting in Kansas City. Bull. Med. Libr. Assoc. 1973; 61:39–43. [PubMed: 16017634]

Dane KY, Nembrini C, Tomei AA, Eby JK, O'Neil CP, Velluto D, Swartz MA, Inverardi L, Hubbell JA. Nano-sized drug-loaded micelles deliver payload to lymph node immune cells and prolong allograft survival. J. Control. Release. 2011; 156:154–160. [PubMed: 21864593]

Flechner SM, Kobashigawa J, Klintmalm G. Calcineurin inhibitor-sparing regimens in solid organ transplantation: focus on improving renal function and nephrotoxicity. Clin. Transplant. 2008; 22:1–15. [PubMed: 18217899]

Goldstein DR, Tesar BM, Akira S, Lakkis FG. Critical role of the Toll-like receptor signal adaptor protein MyD88 in acute allograft rejection. J. Clin. Invest. 2003; 111:1571–1578. [PubMed: 12750407]

Haller M, Oberbauer R. Calcineurin inhibitor minimization, withdrawal and avoidance protocols after kidney transplantation. Transpl. Int. 2009; 22:69–77. [PubMed: 18764837]

Halloran PF. Immunosuppressive drugs for kidney transplantation. N. Engl. J. Med. 2004; 351:2715–2729. [PubMed: 15616206]

Hänninen A, Salmi M, Simell O, Andrew D, Jalkanen S. Recirculation and homing of lymphocyte subsets: dual homing specificity of beta 7-integrin(high)-lymphocytes in nonobese diabetic mice. Blood. 1996; 88:934–944. [PubMed: 8704252]

Hunter Z, McCarthy DP, Yap WT, Harp CT, Getts DR, Shea LD, Miller SD. A biodegradable nanoparticle platform for the induction of antigen-specific immune tolerance for treatment of autoimmune disease. ACS Nano. 2014; 8:2148–2160. [PubMed: 24559284]

Jewell CM, López SC, Irvine DJ. In situ engineering of the lymph node microenvironment via intranodal injection of adjuvant-releasing polymer particles. Proc. Natl. Acad. Sci. USA. 2011; 108:15745–15750. [PubMed: 21896725]

Jones ND, Van Maurik A, Hara M, Gilot BJ, Morris PJ, Wood KJ. T-cell activation, proliferation, and memory after cardiac transplantation in vivo. Ann. Surg. 1999; 229:570–578. [PubMed: 10203092]

Kobayashi H, Turkbey B, Watanabe R, Choyke PL. Cancer drug delivery: considerations in the rational design of nanosized bioconjugates. Bioconjug. Chem. 2014; 25:2093–2100. [PubMed: 25385142]

Kolata G. Drug transforms transplant medicine. Science. 1983; 221:40–42. [PubMed: 6407111]

Krupnick AS, Lin X, Li W, Higashikubo R, Zinselmeyer BH, Hartzler H, Toth K, Ritter JH, Berezin MY, Wang ST, et al. Central memory CD8+ T lymphocytes mediate lung allograft acceptance. J. Clin. Invest. 2014; 124:1130–1143. [PubMed: 24569377]

Lakkis FG, Sayegh MH. Memory T cells: a hurdle to immunologic tolerance. J. Am. Soc. Nephrol. 2003; 14:2402–2410. [PubMed: 12937320]

Lakkis FG, Arakelov A, Konieczny BT, Inoue Y. Immunologic 'ignorance' of vascularized organ transplants in the absence of secondary lymphoid tissue. Nat. Med. 2000; 6:686–688. [PubMed: 10835686]

Liu H, Moynihan KD, Zheng Y, Szeto GL, Li AV, Huang B, Van Egeren DS, Park C, Irvine DJ. Structure-based programming of lymph-node targeting in molecular vaccines. Nature. 2014; 507:519–522. [PubMed: 24531764]

Michie SA, Streeter PR, Bolt PA, Butcher EC, Picker LJ. The human peripheral lymph node vascular addressin. An inducible endothelial antigen involved in lymphocyte homing. Am. J. Pathol. 1993; 143:1688–1698. [PubMed: 8256856]

Mikulowska-Mennis A, Xu B, Berberian JM, Michie SA. Lymphocyte migration to inflamed lacrimal glands is mediated by vascular cell adhesion molecule-1/alpha(4)beta(1) integrin, peripheral node

address in/ l-selectin, and lymphocyte function-associated antigen-1 adhesion pathways. Am. J. Pathol. 2001; 159:671–681. [PubMed: 11485925]

Mitragotri S, Burke PA, Langer R. Overcoming the challenges in administering biopharmaceuticals: formulation and delivery strategies. Nat. Rev. Drug Discov. 2014; 13:655–672. [PubMed: 25103255]

Nel AE, Mädler L, Velegol D, Xia T, Hoek EM, Somasundaran P, Klaessig F, Castranova V, Thompson M. Understanding biophysicochemical interactions at the nano-bio interface. Nat. Mater. 2009; 8:543–557. [PubMed: 19525947]

Ochando JC, Yopp AC, Yang Y, Garin A, Li Y, Boros P, Llodra J, Ding Y, Lira SA, Krieger NR, Bromberg JS. Lymph node occupancy is required for the peripheral development of alloantigen-specific Foxp3+ regulatory T cells. J. Immunol. 2005; 174:6993–7005. [PubMed: 15905542]

Oussoren C, Storm G. Liposomes to target the lymphatics by subcutaneous administration. Adv. Drug Deliv. Rev. 2001; 50:143–156. [PubMed: 11489337]

Park CO, Kupper TS. The emerging role of resident memory T cells in protective immunity and inflammatory disease. Nat. Med. 2015; 21:688–697. [PubMed: 26121195]

Penaranda C, Tang Q, Ruddle NH, Bluestone JA. Prevention of diabetes by FTY720-mediated stabilization of peri-islet tertiary lymphoid organs. Diabetes. 2010; 59:1461–1468. [PubMed: 20299465]

Reddy ST, van der Vlies AJ, Simeoni E, Angeli V, Randolph GJ, O'Neil CP, Lee LK, Swartz MA, Hubbell JA. Exploiting lymphatic transport and complement activation in nanoparticle vaccines. Nat. Biotechnol. 2007; 25:1159–1164. [PubMed: 17873867]

Somers WS, Tang J, Shaw GD, Camphausen RT. Insights into the molecular basis of leukocyte tethering and rolling revealed by structures of P- and E-selectin bound to SLe(X) and PSGL-1. Cell. 2000; 103:467–479. [PubMed: 11081633]

Sperandio M, Gleissner CA, Ley K. Glycosylation in immune cell trafficking. Immunol. Rev. 2009; 230:97–113. [PubMed: 19594631]

Stacker SA, Williams SP, Karnezis T, Shayan R, Fox SB, Achen MG. Lymphangiogenesis and lymphatic vessel remodelling in cancer. Nat. Rev. Cancer. 2014; 14:159–172. [PubMed: 24561443]

Streeter PR, Rouse BT, Butcher EC. Immunohistologic and functional characterization of a vascular addressin involved in lymphocyte homing into peripheral lymph nodes. J. Cell Biol. 1988; 107:1853–1862. [PubMed: 2460470]

Tong R, Cheng J. Paclitaxel-initiated, controlled polymerization of lactide for the formulation of polymeric nanoparticulate delivery vehicles. Angew. Chem. Int. Ed. Engl. 2008; 47:4830–4834. [PubMed: 18491339]

Tong R, Yala L, Fan TM, Cheng J. The formulation of a ptamercoated paclitaxel-polylactide nanoconjugates and their targeting to cancer cells. Biomaterials. 2010; 31:3043–3053. [PubMed: 20122727]

van Zante A, Gauguet JM, Bistrup A, Tsay D, von Andrian UH, Rosen SD. Lymphocyte-HEV interactions in lymph nodes of a sulfotransferase-deficient mouse. J. Exp. Med. 2003; 198:1289–1300. [PubMed: 14597732]

Vercauteren SB, Bosmans JL, Elseviers MM, Verpooten GA, De Broe ME. A meta-analysis and morphological review of cyclosporine-induced nephrotoxicity in auto-immune diseases. Kidney Int. 1998; 54:536–545. [PubMed: 9690221]

Vergani A, Tezza S, D'Addio F, Fotino C, Liu K, Niewczas M, Bassi R, Molano RD, Kleffel S, Petrelli A, et al. Long-term heart transplant survival by targeting the ionotropic purinergic receptor P2×7. Circulation. 2013; 127:463–475. [PubMed: 23250993]

von Andrian UH, Mackay CR. T-cell function and migration. Two sides of the same coin. N. Engl. J. Med. 2000; 343:1020–1034. [PubMed: 11018170]

von Andrian UH, Mempel TR. Homing and cellular traffic in lymph nodes. Nat. Rev. Immunol. 2003; 3:867–878. [PubMed: 14668803]

Wagner V, Dullaart A, Bock AK, Zweck A. The emerging nano-medicine landscape. Nat. Biotechnol. 2006; 24:1211–1217. [PubMed: 17033654]

Wong W, Venetz JP, Tolkoff-Rubin N, Pascual M. 2005 immunosuppressive strategies in kidney transplantation: which role for the calcineurin inhibitors? Transplantation. 2005; 80:289–296. [PubMed: 16082321]

Xu B, Wagner N, Pham LN, Magno V, Shan Z, Butcher EC, Michie SA. Lymphocyte homing to bronchus-associated lymphoidtissue (BALT) is mediated by L-selectin/PNAd, alpha4beta1 integrin/VCAM-1, and LFA-1 adhesion pathways. J. Exp. Med. 2003; 197:1255–1267. [PubMed: 12756264]

Xu B, Cook RE, Michie SA. Alpha4beta7 integrin/MAdCAM-1 adhesion pathway is crucial for B cell migration into pancreatic lymph nodes in nonobese diabetic mice. J. Autoimmun. 2010; 35:124–129. [PubMed: 20488663]

Yeste A, Nadeau M, Burns EJ, Weiner HL, Quintana FJ. Nanoparticle-mediated codelivery of myelin antigen and a tolerogenic small molecule suppresses experimental autoimmune encephalomyelitis. Proc. Natl. Acad. Sci. USA. 2012; 109:11270–11275. [PubMed: 22745170]

Yin N, Zhang N, Xu J, Shi Q, Ding Y, Bromberg JS. Targeting lymphangiogenesis after islet transplantation prolongs islet allograft survival. Transplantation. 2011; 92:25–30. [PubMed: 21508896]

Yuan X, Salama AD, Dong V, Schmitt I, Najafian N, Chandraker A, Akiba H, Yagita H, Sayegh MH. The role of the CD134-CD134 ligand costimulatory pathway in alloimmune responses in vivo. J. Immunol. 2003; 170:2949–2955. [PubMed: 12626546]

Zhang XY, Lu WY. Recent advances in lymphatic targeted drug delivery system for tumor metastasis. Cancer Biol. Med. 2014; 11:247–254. [PubMed: 25610710]

Zhang BW, Zimmer G, Chen J, Ladd D, Li E, Alt FW, Wiederrecht G, Cryan J, O'Neill EA, Seidman CE, et al. T cell responses in calcineurin A alpha-deficient mice. J. Exp. Med. 1996; 183:413–420. [PubMed: 8627154]

In Brief

Azzi et al. show the targeted delivery of microparticles containing tacrolimus to the draining lymph nodes of recipients following organ transplantation via intravenous administration. Microparticles containing tacrolimus coated with an antibody against peripheral lymph node addressin are trafficked to the draining lymph nodes, resulting in a significant prolongation of murine heart allograft survival.

Highlights

- The MECA79 antibody binds peripheral lymph node addressin (PNAd)
- Tacrolimus-loaded microparticles coated with MECA79 target lymph nodes
- Microparticles accumulate in draining lymph nodes after intravenous delivery
- Targeted delivery of tacrolimus prolonged allograft survival

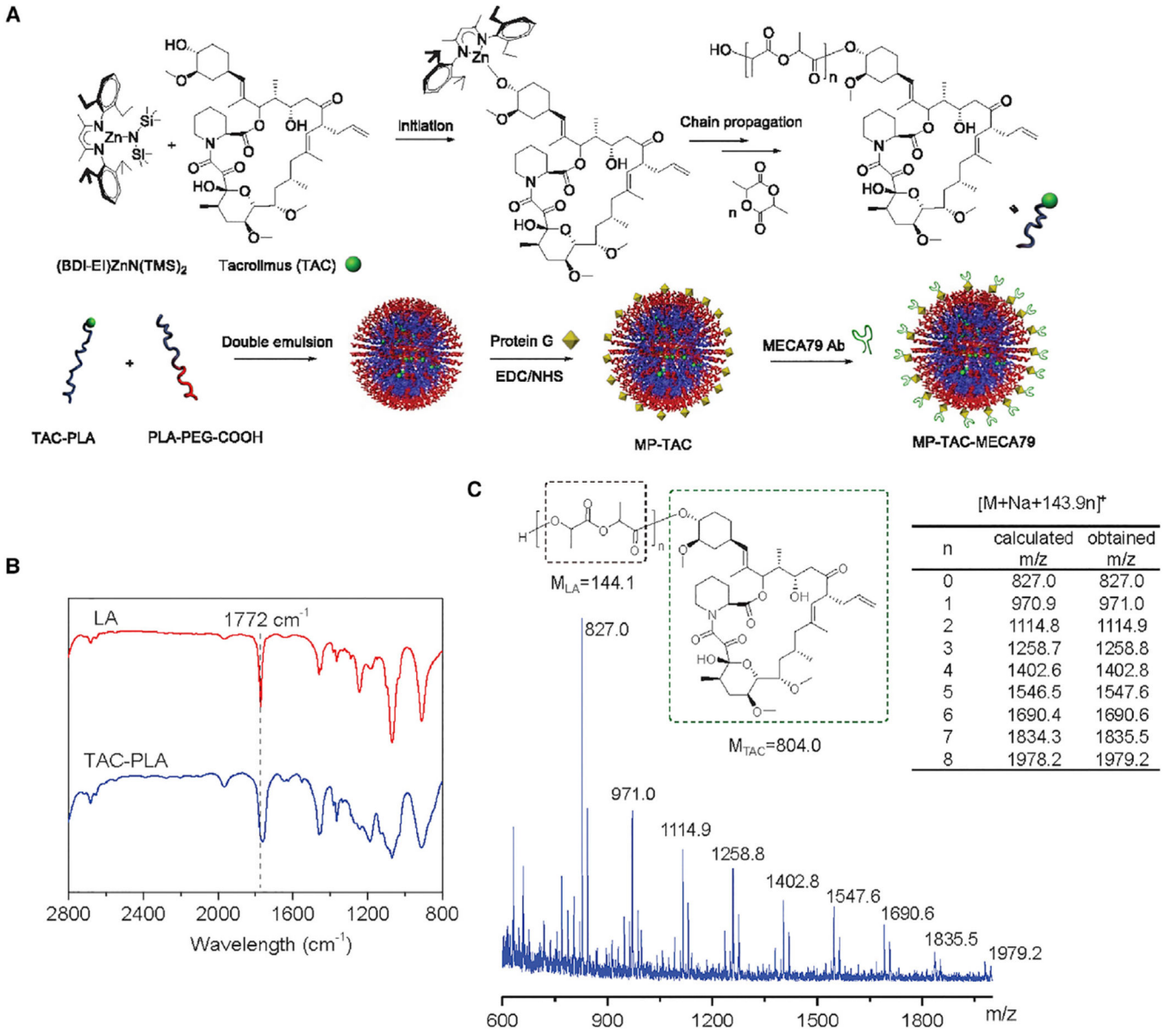

[M+Na+143.9n]+

n	calculated m/z	obtained m/z
0	827.0	827.0
1	970.9	971.0
2	1114.8	1114.9
3	1258.7	1258.8
4	1402.6	1402.8
5	1546.5	1547.6
6	1690.4	1690.6
7	1834.3	1835.5
8	1978.2	1979.2

Figure 1. Preparation of TAC-PLA Polymer Conjugate and Formulation of PEGylated MP-TAC-MECA79 and MP-TAC

(A) Schematic of the synthesis of TAC-PLA polymer conjugate by means of TAC-initiated LA polymerization in the presence of $(BDI\text{-}EI)ZnN(TMS)_2$ catalyst and preparation of MP-TAC-MECA79 with the surface modified by the MECA79 antibody.

(B) FT-IR spectra of LA (red) and TAC-PLA conjugates (blue). The complete conversion of LA was determined via FT-IR by monitoring the disappearance of the band at 1772 cm^{-1}).

(C) MALDI-TOF analysis for TAC-PLA_n conjugates. The obtained mass to charge ratio (m/z) is identical to the calculated m/z of $[TAC\text{-}PLA_n + Na]^+$ (804.0+143.9 × n + 23).

A

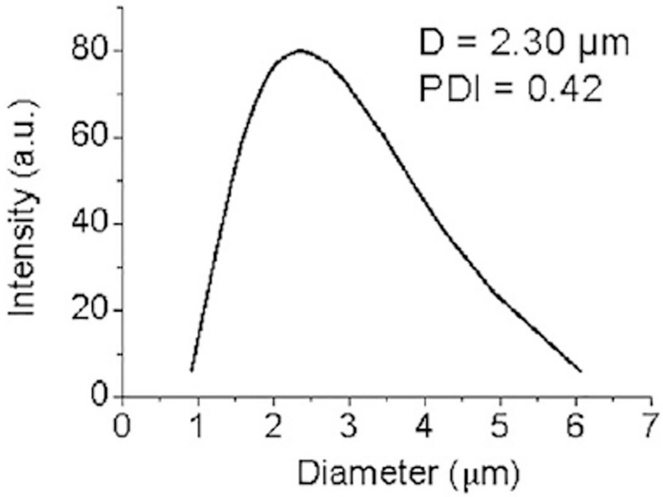

B

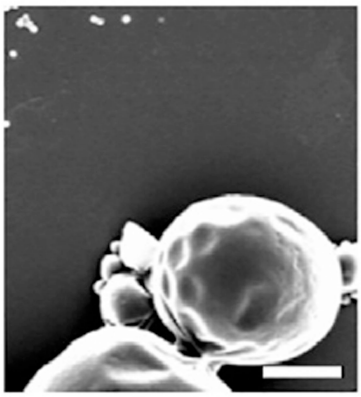

C

Group	MP-TAC-MECA79	MP-TAC
	TAC-PLA/PLA-PEG-protein G /MECA79 Ab	TAC-PLA/PLA-PEG-protein G
M_wPEG (Da)	5k	5k
Drug loading (wt%)	9.1	9.1
Size (µm)	2.30	2.36
PDI	0.42	0.37
Zeta potencial (mV)	-22	-21

D

Group	Before lyophilization		After lyophilization	
	D (µm)	PDI	D (µm)	PDI
MP-TAC	2.36	0.37	3.26	0.43
MP-TAC-MECA79	2.3	0.42	3.16	0.37

Figure 2. Characterization of PEGylated MP-TAC-MECA79 and MP-TAC

(A) DLS measurement of MP-TAC-MECA79. D, average diameter; PDI, polydispersity index.

(B) A representative scanning electron microscope image of PEGylated MP-TAC-MECA79 (scale bar, 1 µm).

(C) Formulation parameters and physicochemical properties of PEGylated MP-TAC-MECA79 and MP-TAC. M_w PEG, molecular weight of poly(ethylene glycol.

(D) Particle sizes and polydispersities of MP-TAC-MECA79 and MP-TAC before and after lyophilization.

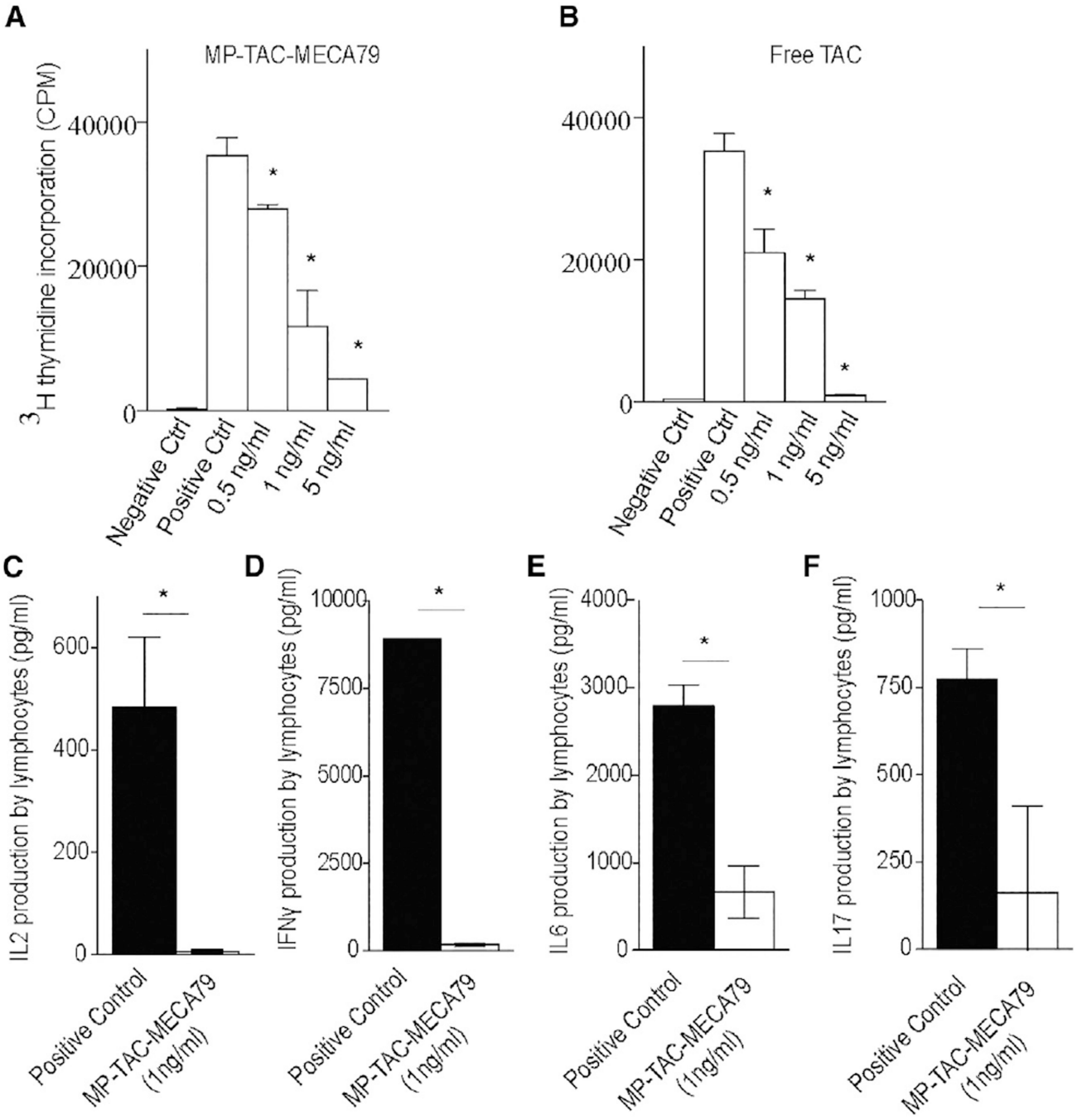

Figure 3. MP-TAC-MECA79 Suppresses T Cell Proliferation in a Dose-Dependent Fashion In Vitro and Suppresses Inflammatory Cytokine Production by T Cells

(A) C57BL/6 splenocytes were stimulated in vitro with anti-CD3 and anti-CD28 antibodies in a flat-bottom plate. MP-TAC-MECA79 was added in escalating doses to the T cell stimulation assay. MP-TAC-MECA79 suppressed T cell proliferation, as measured by thymidine incorporation, in a dose-dependent fashion, starting at 0.5 ng/ml TAC-equivalent concentration (*$p < 0.05$). Ctrl, control, CPM, count per minute.

(B) Free TAC suppressed T cell proliferation, as measured by thymidine incorporation, in a dose-dependent fashion, starting at 0.5 ng/ml TAC-equivalent concentration (*$p < 0.05$).

(C) The suppression of IL2 production by CD3/CD28-stimulated T cells by MP-TAC-MECA79 at a concentration of 1 ng/ml TAC equivalent (*$p < 0.05$).
(D) The suppression of IFNγ production by CD3/CD28-stimulated T cells by MP-TAC-MECA79 at a concentration of 1 ng/ml TAC equivalent (*$p < 0.05$).
(E) The suppression of IL6 production by CD3/CD28-stimulated T cells by MP-TAC-MECA79 at a concentration of 1 ng/ml TAC equivalent (*$p < 0.05$).
(F) The suppression of IL17 production by CD3/CD28-stimulated T cells by MP-TAC-MECA79 at a concentration of 1 ng/ml TAC equivalent (*$p < 0.05$).

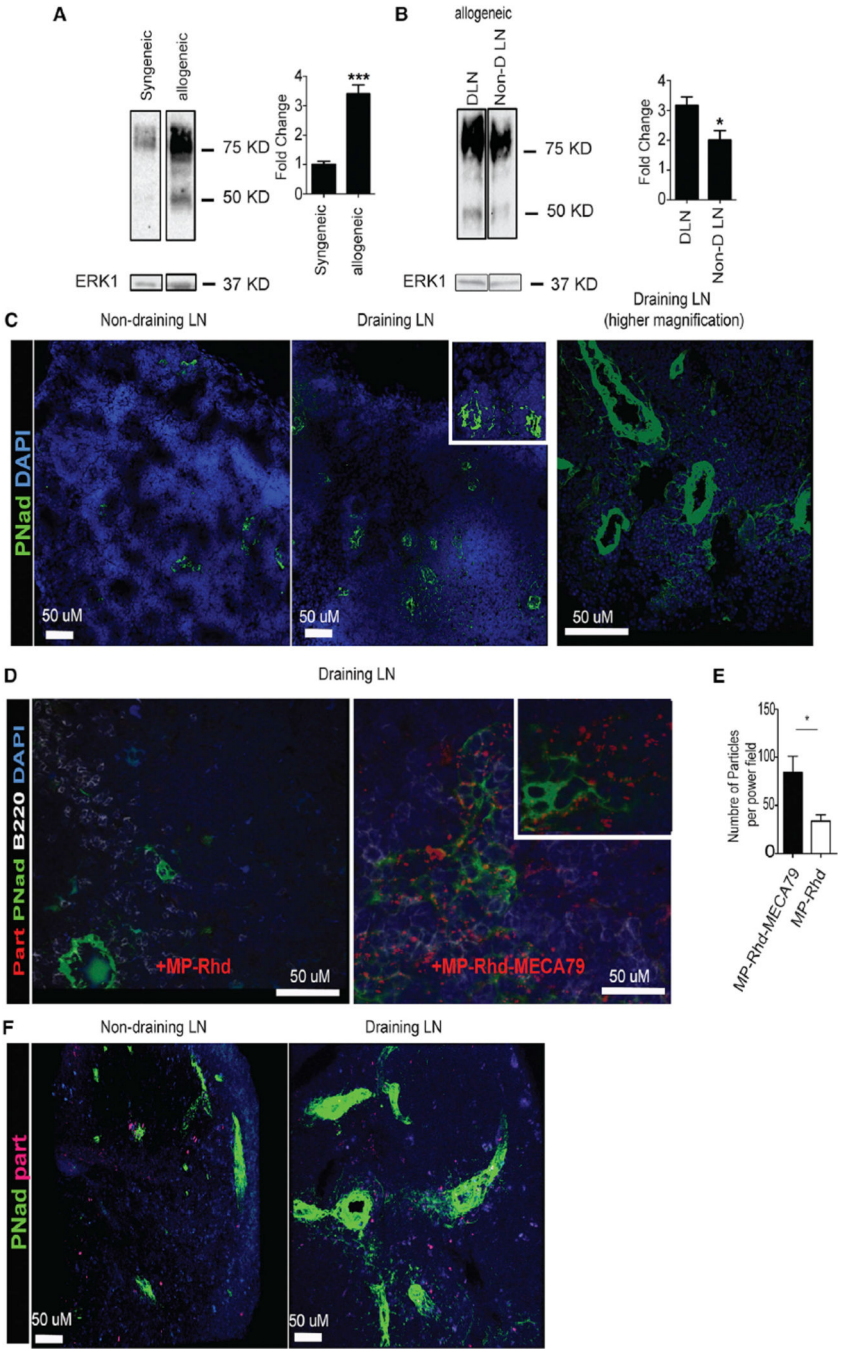

Figure 4. Increased Expression of PNAd in DLNs Facilitates Targeted Delivery of MP-MECA79 in a Transplant Mouse Model

(A) Western blot analysis of cell suspensions from the DLNs of mice transplanted with syngeneic or allogeneic skin grafts showed a 4-fold increase in PNAd expression in allogeneic compared with syngeneic transplants. Total ERK1 was used as a loading control. The fold change over the syngeneic sample was calculated after densitometric analysis and correction for ERK1 (***$p < 0.001$).

(B) Western blot analysis of cell suspensions from the DLNs and non-DLNs of mice transplanted with allogeneic skin grafts showed significant increases in PNAd expression in

DLNs compared with non-DLNs. The fold change over the non-DLN sample was calculated after densitometric analysis and correction for ERK1 (*$p < 0.05$).

(C) DLNs of mice transplanted with allogeneic skin grafts were analyzed by immunohistochemistry after intravenous injection of rhodamine-labeled MP-TAC-MECA79 (MP-Rhd-MECA79) or MP-TAC (MP-Rhd). DLN showed greatly increased PNAd (arrows) compared with non-draining LNs (pancreatic LNs). A 20× objective was used. Further extension of PNAd-positive cells from much larger vessels in the DLNs was also observed (left). A 40× objective was used.

(D) MECA79 particles but not control particles are localized to adjacent spaces of PNAd-positive endothelial cells in the DLNs. Many MECA79 particles are lined up by PNAd. The cell nuclei were visualized by DAPI. A 40× objective was used.

(E) A higher number of particles was counted per high-power field (200×) in DLNs isolated from mice treated with MP-Rhd-MECA79 compared with MP-Rhd (*$p < 0.05$, $n = 4$ mice/group).

(F) Two-photon imaging shows greatly increased PNAd expression (green) in DLNs compared with non-draining LNs. A higher number of MP-Rhd-MECA79 is observed in the DLNs compared with the non-draining LNs.

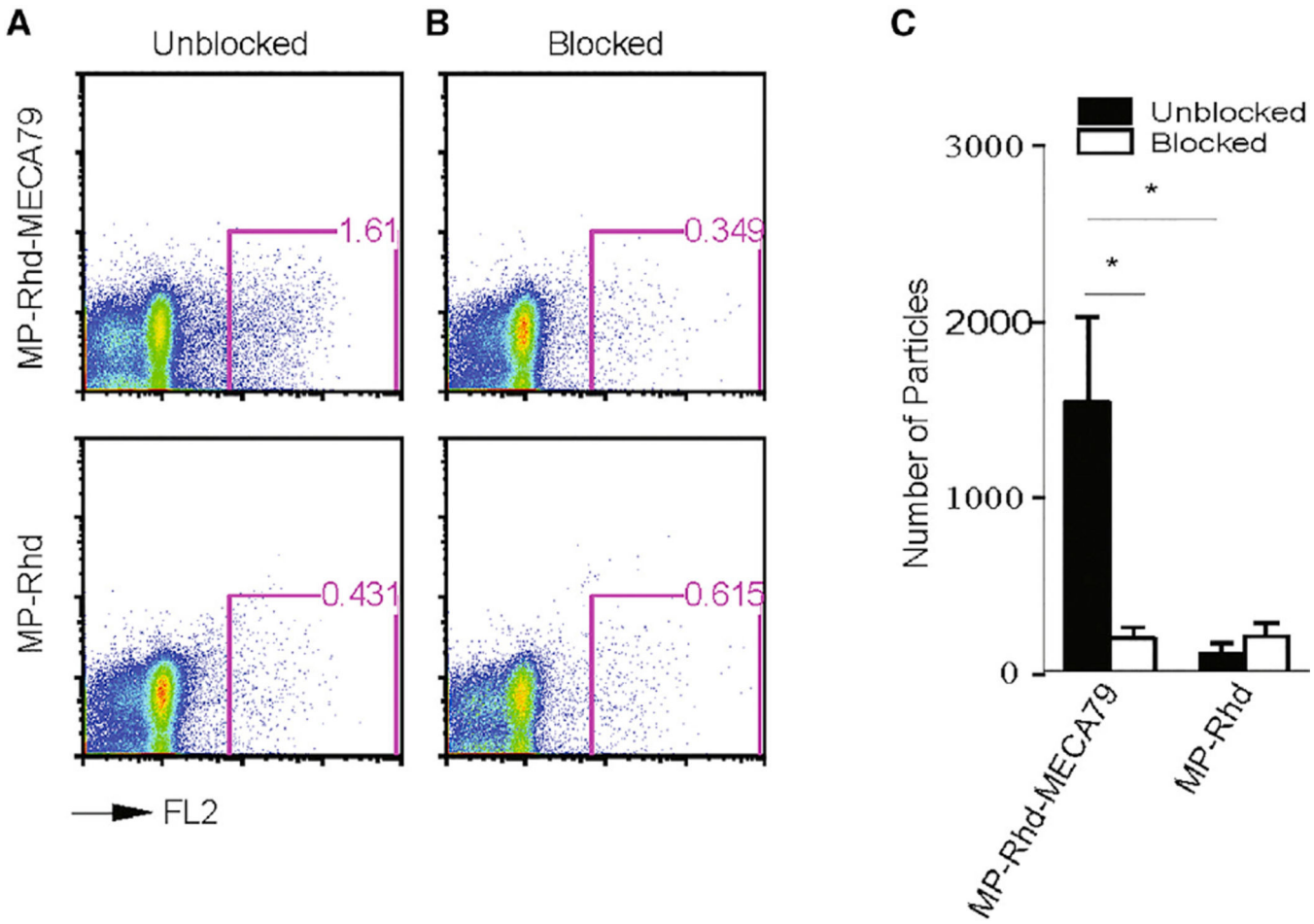

Figure 5. Blocking PNAd Reduces Targeted Delivery of MP-MECA79 in a Transplant Mouse Model

(A) FACS analysis of cell suspension from the inguinal DLNs of skin transplant recipients injected with either MP-Rhd-MECA79 or MP-Rhd, showing a greater accumulation of rhodamine-labeled MP-MECA79 compared with MPs.

(B) FACS analysis of cell suspension from the DLNs of skin transplant recipients injected with blocking anti-PNAd antibody 1 hr before injection of rhodamine-labeled particles.

(C) The absolute number of rhodamine-labeled particles in the four different groups of mice ($n = 4$ mice /group, $*p < 0.05$).

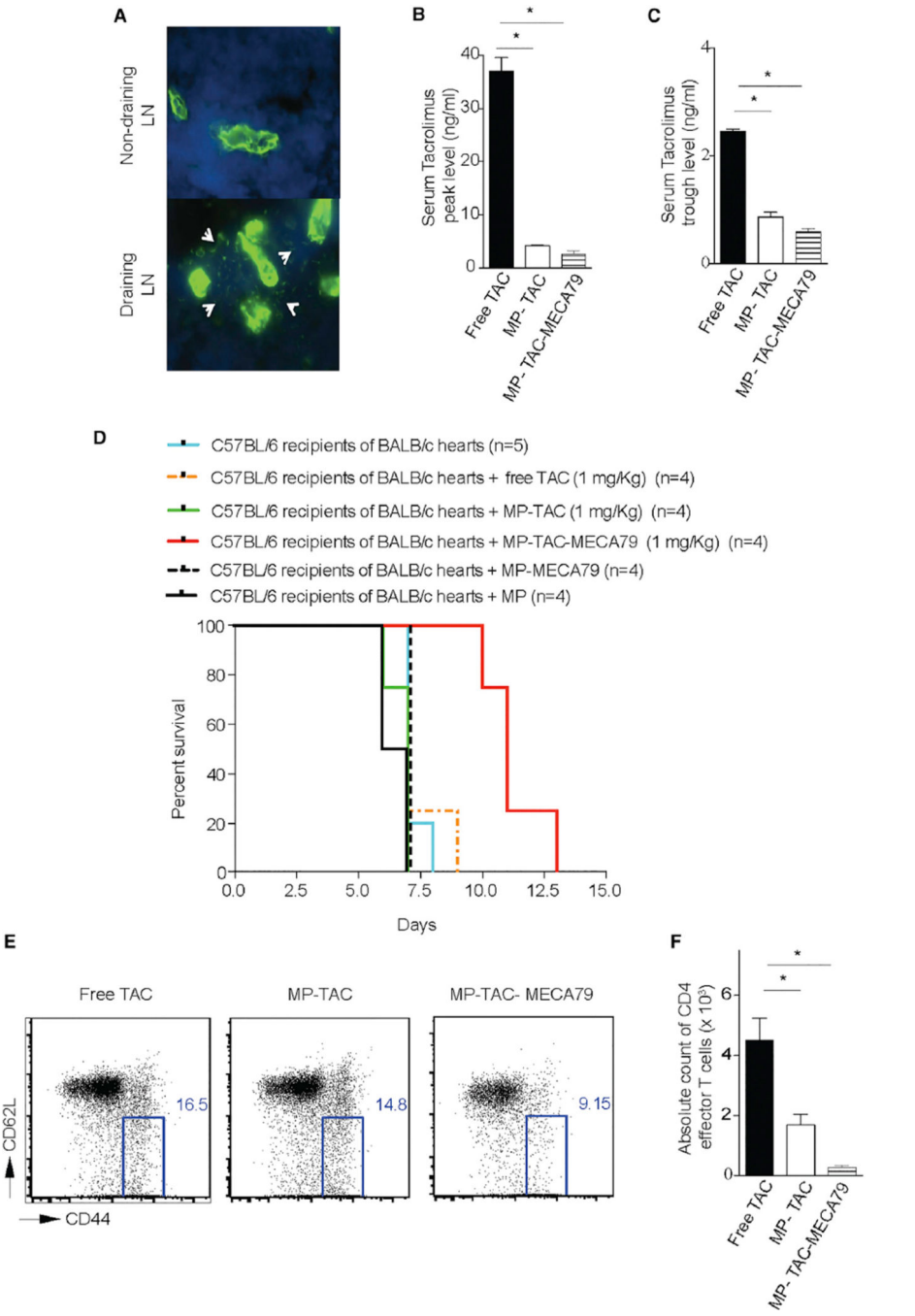

Figure 6. MP-TAC-MECA79 Prolongs Heart Allograft Survival in Mice with Lower Serum Peak and Trough TAC Levels Compared with the Free TAC Group

(A) Immunohistochemistry analysis of the DLN of mice transplanted with heart allografts showed an increase in PNAd expression compared with non-draining LNs (axillary LNs) on day 7 post-transplantation. A 20× objective was used. Further extension of PNAd-positive cells from much larger vessels in the DLNs was also observed, giving a mesh-like appearance (arrows).

(B) C57BL/6 mouse recipients of fully mismatched BALB/c hearts were injected daily via the tail vein with either MP-TAC-MECA79, MP-TAC, MP-MECA79, or free TAC at 1

mg/kg TAC equivalent. The TAC level was measured in the peripheral blood of the transplanted mice on day 3 after transplantation. The graph shows that the peak TAC level 2 hr after injection of the compounds was significantly lower for MP-TAC-MECA79 compared with free TAC (*$p < 0.05$, n = 4 mice/group).

(C) The TAC trough level 24 hr after injection was significantly lower for MP-TAC-MECA79 compared with free TAC (*$p < 0.05$).

(D) Kaplan-Meier survival curve of heart allograft recipients treated with MP-TAC-MECA79. C57BL/6 mouse recipients of fully mismatched BALB/c hearts were injected daily via the tail vein with either MP-TAC-MECA79, MP-TAC, MP, MP-MECA79, or free TAC at 1 mg/kg TAC equivalent. Compared with the other groups, treating recipients with MP-TAC-MECA79 significantly increased heart allograft survival (median survival 7 versus 7 versus 7 versus 11 days, respectively; n = 4/group; $p < 0.05$).

(E) FACS analysis of DLNs from heart transplant recipients treated with either MP-TAC-MECA79, MP-TAC, or free TAC showing a significant reduction in the percentage of effector CD4 T cells ($CD4^{+}CD62L^{low}CD44^{high}$) in DLNs of mice treated with MP-TAC-MECA79 compared with the MP-TAC- or free TAC-treated groups.

(F) The absolute count of CD4 effector T cells in the DLNs of the three different groups of transplanted mice shows a significantly lower number of CD4 effector T cells in the DLNs of mice treated with MP-TAC-MECA79 compared with mice treated with MP-TAC or free TAC (*$p < 0.05$, n = 3–4 mice/group).